STRUCTURAL, OPTICAL AND TEMPERATURE DEPENDENT DIELECTRIC STUDY OF ZINC OXIDE (ZnO) INCORPORATED MAGNESIUM OXIDE (MgO) BASED COMPOUNDS

SYNOPSIS

Submitted in partial fulfilment of the requirements for the award of the degree of
Doctorate of Philosophy
in
Physics

Submitted by

Jyotsna
Enrollment No.: H13959

Under the supervision of

Dr. Rajender Kumar
Associate Professor

DEPARTMENT OF PHYSICS
SCHOOL OF BASIC AND APPLIED SCIENCES
CAREER POINT UNIVERSITY HAMIRPUR
TIKKER (KHARWARIAN), BHORANJ
HAMIRPUR (HP)-176041, INDIA

2021-22

INTRODUCTION

1.1 COMPOUND SEMICONDUCTORS

The technological predominance of the semiconductor device industry is pervasive, and technological innovation will be crucial to its growth. Integrating nanostructures with traditional materials opens up opportunities for next-generation electronic and optoelectronic devices (Hanish et al., 2020; Obeid et al., 2018; Sun et al., 2016). In the present scenario of continuous scaling of devices, high-*k* dielectric metal oxide nanomaterials, such as titanium dioxide (TiO_2) and zirconium dioxide (ZrO_2), are at the forefront of modern semiconductor technology and have grabbed the attention of academicians and technologists for exploring their potential in technological advancements. In this regard, metal oxide nanomaterials with insulating nature and high dielectric constant (k >7) are rigorously researched to replace the near-perfect insulating dielectric SiO_2 (k ~ 3.9) interlayer in metal-insulator-semiconductor (MIS) devices to meet the recent trends of miniaturization of devices and to reduce the leakage current issues. High *k*-dielectric metal oxides offer a competitive advantage over materials with low dielectric constant by eliminating the constraint of dielectric thickness (Kwo et al., 2003; Sharma et al., 2022).

The II-VI compounds, such as zinc oxide (ZnO) and cadmium oxide (CdO), are among the most preferred materials that manifest incredible potential in the realm of diverse fields like electronics, medicine, energy storage, sensors and coatings, etc., offering myriad possibilities for enhancing their performance. These multifunctional materials with direct wide bandgap, high melting point, high electrical resistivity, low intrinsic carrier concentration, and large exciton binding energy make them very attractive for electronic and optoelectronic device applications. Rigorous research on these materials has provided more profound insight into their fundamental and application aspects. In nanostructured forms, these compounds prove their metal in diverse applications such as photocatalysis, gas sensing, antibacterial, toxic waste remedial, lighting, and display. Nevertheless, the sluggish progress in improving the efficacy of electronic devices, owing to the challenges, such as the need for suitable materials with defect engineering and doping mechanisms, requires revisiting the material processing at the fundamental level. Effective exploitation of these compound semiconductor nanostructures is possible by improving their dielectric constant, defect and bandgap engineering using some suitable dopant.

According to Robertson (2004), high-*k* materials with wide bandgaps (insulating properties) and minimal defects are apt to meet the criteria for a suitable interlayer in a MIS device for enhanced performance. Its high dielectric constant is required to achieve smaller equivalent oxide thickness (EOT), wide bandgap to have a suitable conduction/valence band offset for providing effective barriers to the charge carriers to take care of inexorable leakage current issues and lower defect density to avoid trapping of charge carriers (Lu, H. & Zhang, D.W., 2012). In this direction, some oxide materials ($SrTiO_3$, $BaTiO_3$, and TiO2) with colossal permittivity have been explored for their applications in these electronic devices. However, their significant dielectric loss and considerable frequency and temperature dependence restricted their applications. The strong temperature-dependent behavior affects their capacitive and conducting properties and, in turn, significantly constricts the operational temperature range of the devices.

1.2 METAL OXIDES

Compound semiconductors, especially metal oxides, have drawn attention due to their versatility in terms of their insulating, semiconducting, metallic or even superconducting behavior as they can possess varied electronic properties (D'Souza et al., 2007). These multifunctional materials display numerous unique properties such as luminescence, magnetism, dielectric, thermoelectric, chemical and thermal stability, which propose an implausible prospect for developing cutting-edge electronic device technologies. Metal oxides are imperative for progress in energy storage, microelectronics, optoelectronics, sensing and catalysis. The suitability of these materials is revealed by the rigorous research activities that are being undertaken to determine their diverse applications. Metal oxides are divided into three categories based on the type of metal, such as ceramic oxides (COs), transition metal oxides (TMOs), and rare earth metal oxides (REMOs).

Ceramic oxides are the inorganic oxides of metals or metalloids such as MgO and Al_2O_3 that possess high melting points, excellent mechanical properties, low wear resistance, and high corrosion resistance. Due to these wonderful properties, oxide ceramics find applications in diverse fields like biomedical, anti-corrosive coatings, refractory and electrical insulation (Lee et al., 2023; Tamizh et al., 2014; Wilson, I.O., 1981).

Transition metal oxides exhibit unique properties due to their partially filled d-subshells. They can have variable oxidation states owing to which they display excellent

diverse magnetic properties such as paramagnetic, ferromagnetic and ferromagnetic. Examples of TMOs include NiO, ZnO and MnO_2. The multiple oxidation states of these oxides result in enhanced redox reactions, making them suitable electrode material. Moreover, they exhibit good luminescent properties and hence find applications in optoelectronics (Balamurugan & Mehta, 2001; Desai et al., 2023; Hafef et al., 2017; Saadi et al., 2023).

Rare earth elements include 17 elements, lanthanides, yttrium and scandium. Most of the applications of these materials are in the form of oxides because of their unique properties. They have been widely used as additives in metal alloys for metallurgical applications, lighting device applications, ceramics, batteries and solid oxide fuel cells and also have biomedical applications. REMOs like HfO_2, ZrO_2, La_2O_3, Y_2O_3 etc. are high-k materials with wide bandgap and have attracted considerable attention for applications as an alternative gate dielectric material in MIS/MOS devices to address the leakage current problems. These materials also have the potential to relax the constraints regarding equivalent oxide thickness (EOT) for the continuous scaling process (Hsieh et al., 2019; Wang et al., 2022).

Since past four decades intense research on high-*k* materials such as metal oxides like ZnO, TiO_2, In_2O_3, rare earth metal oxides such as zirconium dioxide (ZrO_2), yttrium oxide (Y_2O_3), hafnium oxide (HfO_2), lanthanum oxide (La_2O_3), gadolinium oxide (Gd_2O_3), praseodymium oxide (Pr_6O_{11}) and organic polymers such as doped polyvinyl alcohol (PVA), maleic anhydride have reported them as efficient insulators in MIS devices. These studies have established that a high-*k* insulating layer in MIS device guarantees a good rectifying nature, lower reverse leakage current, higher barrier height and lower interface state density compared to the MS diode (Prasad et al., 2017) and that the parameters that control the efficiency of MIS device include thickness and homogeneity of the interfacial layer, density of the interface states (Nss) at the interface and the series resistance (Rs). Further, rigorous investigations are desirable to take care of the operational instabilities and enhance the performance of the device.

In the current state of the art, there is a considerable focus on synthesizing engineered insulating metal oxides with high-*k*, low loss, reduced defects, high resistivity and feeble temperature-dependent behavior of its conductivity, which can play a vital role in addressing the aforementioned problems in MIS electronic devices to meet the requirements of the continuous scaling process. With this motivation, the present study focuses on creating a suitable raw material exhibiting the above properties by

engineering the insulating metal oxide (MgO) via composition-controlled doping and variation of synthesis conditions. A detailed structural, optical and dielectric investigation will enable us to ascertain their feasibility and suitability to act as an insulating interlayer in MIS devices with enhanced performance. However, realizing some of the desired parameters can render other parameters critical. In this direction, material engineering holds the potential for numerous improvements simultaneously and supports ongoing research in diverse fields.

1.3 METAL OXIDES CHOSEN IN PRESENT WORK

In this work, a ceramic oxide (magnesium oxide) as a host material and a transition metal oxide (zinc oxide) as a dopant have been chosen to synthesize metal oxide nanocomposites and doped nanomaterials.

1.3.1 MAGNESIUM OXIDE

Magnesium oxide stands out as a promising candidate for electronic device technology, thanks to its unique properties that ensure the efficient operation of devices. It is one of the most abundant non-toxic metal oxides found on earth's surface with a high melting point (~2852 °C) that addresses the thermal stability issues of the device. MgO is chemically stable and does not react with Si substrate, making it a preferred choice for Si-based microelectronic applications. In earlier reported works, MgO has been successfully deposited on various substrates, such as GaN, MoS_2, ZnO, even Si. The crystal structure of MgO has been reported to be cubic with FCC lattice. Many works have investigated the microstructural, optical and dielectric properties of MgO nanostructures, which reported an improvement in the properties mentioned above due to the large surface-to-volume ratio (Hwang & Chang, 2022; Kaneko et al., 2011).

Magnesium oxide is a highly ionic insulating crystalline metal oxide with a direct bandgap of ~7.8 eV that displays unique properties that make it an attractive choice for a wide range of applications such as in optoelectronics, high-speed switching devices, UV detectors, biosensors, supercapacitors, medicines and toxic waste remedies (Chinthala et al., 2021). Its small refractive index of ~1.735, makes it an appropriate buffer material for optical waveguide applications (Chen et al., 2002). It is a crucial refractory ceramic material with a low dielectric constant (~9.8), limiting its applications in capacitive and energy storage devices. So, recently various strategies like nanostructuring the materials/and doping with metals/metal oxides to form either composites/or solid solutions have been explored to increase its dielectric constant. The dielectric properties

of MgO are highly dependent upon its optical properties, as photo luminescence studies give us an idea of the various defects responsible for trapping and storing the bound charge in a dielectric insulator. The optical properties of magnesium oxide have already been widely studied, and many reports on highly luminescent nanostructured pure and doped forms of MgO are available in the literature. They suggest its applications in optoelectronic devices such as white LED, Yellow or blue LED, display and lighting applications (Sharma & Jeevanandam, 2015; Vasanthi et al., 2017).

Most of the studies of these oxides have been carried out either at room temperature or at temperatures below room temperature. However, for high-temperature applications, the dielectric behavior of these materials needs to be explored at higher temperatures. High-temperature dielectrics are crucial for power systems and energy storage devices operating in harsh ambient conditions. Though tremendous developments are being reported in this field, there is still plenty of scope for advancements in resolving their shortcomings of underperformance. Suitable oxide dielectric materials in nano-form coupled with the doping phenomenon can enhance the performance of electronic devices.

1.3.2 ZINC OXIDE

Zinc oxide is a non-toxic transition metal oxide with a wide bandgap (3.37 eV), varied growth morphologies and a large exciton binding energy (~60 meV). It possesses exciting properties like excellent luminescence and transparency that are manifestations of its wide band gap, admirable quantum efficiency due to high order of charge mobility ($\mu\sim$ 200–300 $cm^2\ V^{-1}\ s^{-1}$) and ferromagnetism due to its large exciton energy. Its high melting point and low thermal expansion mark its application for ceramics, and due to these exotic properties, it can sustain in high-temperature conditions. Moreover, it can also withstand high electric fields due to its wide bandgap (Kaur et al., 2021).

2. LITERATURE REVIEW

A literature survey was conducted in this field to get closer to the objective of this research.

Narayan et al. (2001) reported the synthesis of a novel single-phase cubic alloy $Zn_xMg_{1-x}O$ that has been deposited epitaxially on different substrates by PLD. Deposition on the MgO (100) substrate was done via lattice-matching epitaxy, whereas on Si (100), it was done via domain-matching epitaxy. Titanium nitride (TiN) was used as a buffer layer for alloy deposition on Si substrate due to the large lattice mismatch

(22%) between MgO and silicon substrate. The alloy film with x=0.18 has been observed to be a wide bandgap material. These alloys were explored for their probable applications for UV-based optical devices.

Pacchioni (2001) suggested that excitation wavelengths corresponding to F-centers (O-vacancies) in MgO depend upon their location sites in the lattice. For example, F-centers in bulk MgO (6-coordinated F and F^+) have $\lambda_{ex} \sim$ 250 nm and for surface sites: terrace F-centers (5-coordinated F and F^+) have $\lambda_{ex} \sim$ 410 nm, edge F-centers (4-coordinated F and F^+) have $\lambda_{ex} \sim$ 495–560 nm, corner F-centers (3-coordinated F and F^+) have $\lambda_{ex} \sim$ 560-590 nm. Transitions observed above 600 nm generally do not correspond to F-centers. Nanoparticles of MgO have more pronounced surface effects due to large surface-to-volume ratio as compared to bulk MgO and hence have additional states in its bandgap that lower the gap between CBM and VBM.

Sushko et al. (2002) conducted the theoretical study using an embedded cluster model and DFT to calculate parameters like ionization potential (IP), electron affinity (EA) and optical excitation energies at various low coordinated sites of MgO (100) surface, which depicted their charge trapping probabilities to cause localized charge states. Based on these calculations, the authors reported that holes preferably localize at 3C (corner) O-ions, whereas electrons rather localize at 3C Mg-ions even if they are delocalized at terraces and edges due to their lower energies at 3C sites. They also calculated the optical excitation energies of defects in these low-coordinated sites. The deep-level traps, which include O^{2-} ions (at terrace, edge, and corner), have EA more than 2 eV, whereas shallow traps have EA 1–2 eV. Knowledge concerning the excitation of a definite surface location on irradiation with a specific photon excitation wavelength is necessary for understanding the modulated surface features and transport mechanisms via electronic properties in the doped samples. The dependence of excitation energies on coordination no. of surface O-ions in MgO has been discussed. The excited states in CB and surface terrace sites can transfer charge to low-coordinated sites, causing luminescence. These may help acquire information regarding the excitation of a specific surface site at a particular photon excitation energy.

Chen et al. (2002) utilized the PLD technique to obtain epitaxial MgO (100)/ Si (100) and pure (111) and (110) oriented MgO films on Si (100) by varying ambient temperature and O_2 pressure conditions. The author mentioned that during the early deposition phase, the substrate temperature controls the crystal orientation and has been

ascribed to the equilibrium between surface and boundary energies. During the deposition process, O_2 pressure decides the crystalline quality based on the nucleation process. The etching of the substrate affects the granular structures, which depend upon the mobility of ad atoms.

Robertson (2004) presented a review that discussed the criterion for selecting a high-k dielectric oxide material to replace SiO_2 interlayer in electronic devices in terms of their electronic structures, band offsets, interfacial properties, and electronic defects to take care of continuous scaling of a complementary metal oxide semiconductor (CMOS) device. The author also discussed their capacitive application in dynamic random access memories (DRAM).

Panin et al. (2005) synthesized ZnO/MgO nanostructures using the solution method and studied the effects of annealing temperature on their structure and optical properties. The author reported that on increasing the temperature from 400 °C to 1000 °C, the particle size decreased (10–100) nm, and the bandgap increased related to quantum confinement effects. ZnO–MgO materials started interacting at temperatures above 600 °C, and solid solutions were reportedly formed. Cathode luminescence (CL) spectra revealed a blue shift in the near band edge emission with increase in annealing temperature above 600 °C.

Stankic et al. (2005) studied the size-dependent absorption and luminescent properties of MgO nanosized cubes synthesized by CVD. A blue shift in absorption peaks with increasing particle size has been reported, correlated with the relative concentration of corner and edge ions in these nanocubes of size in the range ~ 3–10 nm. Two absorption peaks at 238 and 281 nm have been observed for particles of 3 nm size, attributed to the excitation of 4-coordinated edge O- ions and 3-coordinated corner O- ions, respectively. With the increase in particle size, the absorption peak corresponding to 3C corner ions decreased, which indicated the lower concentration of corner ions in larger particles. Further, the emission spectrum at excitation wavelength 240 nm displayed an intense emission peak at 370 nm, and a Stokes shift of 1.8 eV was also reported. The emission peak suffered a redshift (~ 380 nm) on increasing the excitation wavelength to 270 nm.

Zhu & Lu (2006) discussed the effect of changing deposition parameters on the orientation of MgO film on Si (100) substrate deposited by PLD. An increase in the ambient O_2 pressure (0.1–200 mTorr) and a decrease in laser fluence (7–3 J/cm^{-2})changed the orientation of the MgO thin film from (111) to (100) and nearly an

epitaxial MgO (100)/ Si (100) was reported at 3 J/cm^{-2} in this work. However, at larger laser fluence (7 J/cm^{-2}), mixed orientations of (111) and (100) were obtained, which were not affected by substrate temperature. Smooth and crack-free MgO films deposited at substrate temperature 400 °C and laser fluence 5 J/cm^{-2} were considered appropriate as buffer layers for the ensuing growth of over layers.

D'Souza et al. (2007) discussed different synthesis methods adopted by the scientific community to obtain various crystalline forms of metal oxides (single crystalline, polycrystalline powder, nanocrystalline, or thin films) in order to realize the desired properties for a particular application. Out of the various compounds, oxides seek the foremost attention due to their versatile nature. Earlier synthesis methods for metal oxides required high temperatures (1000–3000 °C), resulting in materials with low surface area, which restricted their applications in catalysis and sensing. The latest advanced methodologies have led to the production of nanostructured materials with large surface areas even at moderate temperatures, enhancing their sensing and catalytic abilities due to more reaction sites.

Ohira et al. (2008) reported the synthesis of Zn-doped MgO powders by solid-state reaction by varying molar concentrations of ZnO in MgO. An increase in dopant concentration enhanced the UV absorption intensity and the antibacterial property of MgO. This work suggested that the improvement in antibacterial properties might be correlated to the optical absorption phenomenon in synthesized samples. Moreover, the samples with higher ZnO concentrations were reported to be hydration resistant, which can also be useful in applications where moisture can prove to be detrimental.

Baranov et al. (2008) reported ZnO/MgO nanocomposites synthesized by adopting co-precipitation of alcoholic solutions of zinc acetate and magnesium. Bi-phase nanocomposites were obtained at temperatures below 500 °C and solid solutions above 600 °C. CL studies indicated a blue shift in the ZnO excitonic peak with an increase in temperature. Moreover, at 500 °C, a decrease in the intensity of excitonic emission and an increase in the intensity of green emission have been assigned to higher defect density and interfacial interaction between ZnO and MgO host. No excitonic peak was observed at 600 °C, whereas at 700 °C, a blue-shifted UV excitonic peak appeared that indicated the alloy formation.

Chawla et al. (2008) synthesized ZnO/MgO nanocomposites using a solid-state reaction technique and sintered at 1200 °C in the atmosphere of ammonia and nitrogen gases. The ZnMgO alloys are reported to be suitable for applications in photonic devices.

Time-resolved decay studies of photoluminescence in ZnO/MgO indicated the decay times of luminescence on a time scale of 10–100 μs during which excitation, redistribution in trap states, and recombination of charge carriers took place.

Qin et al. (2009) synthesized MgO nanomaterial with hollow tubular tetrapod morphology by developing a ZnO template followed by thermal evaporation of magnesium metal. The synthesized MgO nanomaterial exhibited sharp blue emission peaks in the PL spectrum. In this process, the progression of the tubular MgO phase is accompanied by loss of the ZnO phase, as evident from PL studies where ZnO-specific UV and green emissions were replaced by strong MgO-specific blue emission.

Rajesh Kumar & Subba Rao (2011) reviewed the feasibility of high-k dielectric thin films of various metal oxides for gate dielectric applications in CMOS devices. The high-k metal oxides with large conduction offsets (1.5–3.0 eV) have been suggested as preferable materials. In the case of CMOS devices, the scaling of gate dielectric below 0.18 μm poses an integration problem due to the onset of direct tunneling and issues of gate reliability. So, the research focused on exploring diverse existing and novel metal oxides to accomplish the desired properties of reduced leakage current and power consumption in CMOS devices for enhanced performance.

Selvam et al. (2011) synthesized MgO nanostructures by microwave-assisted combustion method and correlated optical properties with lattice parameters. The enhanced PL emissions in MgO nanostructures compared to MgO micro cubes synthesized by conventional method implied more structural defects in nanostructures due to rapid combustion. On exciting with wavelength 385 nm, a broad emission band in the visible region was observed due to the surface defects, whereas no UV excitonic emission was perceived. The transition $^3B_{1u} \rightarrow {}^1A_g$ related to F_2^{2+} center in D_{2h} symmetry results in an emission band at 437 nm.

Kumar et al. (2011) reported that the photoemission peaks in MgO PL spectrum for $\lambda_{ex} \sim 250$ nm lie in the range 385–460 nm due to 3C corner sites and 335–385 nm due to 4C edge sites. The observed PL spectra in MgO can be assigned to F-centers in MgO and charge transfer at low coordination sites. Even the transitions corresponding to F aggregates (F_2^+, F_2^{2+}, and F_2^{3+}) have been reported in some works.

Rodnyi & Khodyuk (2011) reviewed the optical and luminescent properties of different forms of ZnO, i.e., its single/nanocrystal forms, powder forms, and thin films, to get glimpses of its diverse applications. In this work, the factors that affect the spectral range of the two major emission bands of ZnO in UV and visible regions have been

discussed to enable the researchers to tune these parameters to obtain the desired properties corresponding to a particular application. The choice of dopant, synthesis conditions, and handling of the final product are crucial for altering the optical properties and luminescence of ZnO. Additionally, the desired properties for its application as a scintillator material were explored and discussed.

Mulroue & Duffy (2011) used plane wave DFT to study the properties of different charge states of oxygen defects (vacancies and interstitials) in MgO. It was reported that formation and migration energies, along with other properties, are highly dependent upon the nature of defect charge state. The oxygen vacancies with no trapped electrons (F^{2+}) have lower migration energies as compared to vacancies with trapped electrons (F^{o} and F^{1+}), whereas oxygen interstitials with one trapped hole (O^{1-}) have the lower migration energy (~0.06 eV) as compared to oxygen interstitial with trapped holes (O^{o} and O^{2-}).

Sternig et al. (2012) irradiated MgO nanopowder with two different excitation wavelengths, 240 and 270 nm. The UV photons with wavelength ~240 nm were observed to be efficient for exciting ions at MgO edges, whereas photons with wavelength ~270 nm absorbed effectively at corner sites. The chemical reactivity of the corner and edge sites towards molecular hydrogen was probed regarding the separation of surface excitons at these respective sites. Through PL study, it was reported that edge exciton separation increased considerably in the presence of hydrogen.

Adhlakha et al. (2012) reported the synthesis of mixed-phase ZnO/MgO composites by solid-state reaction method with 35%, 40%, 45%, and 50% MgO in the ZnO host. With increasing concentration of MgO, lattice shrinkage along the c-axis and enhancement in bandgap from 3.16–3.55 eV have been observed. In the photoluminescence spectra, both UV exciton and defect-state emissions were observed, which shifted towards higher energy with an increase in MgO dopant. Magnetic properties were reported to be enhanced with MgO doping.

Athar et al. (2012) synthesized MgO nanoparticles by the non-aqueous sol-gel method at a calcination temperature of 550 °C. This method is advantageous over other methods in controlling the reaction mechanism at the molecular level and in providing a high yield of about 85%. This process can be suitable for large-scale production of MgO nanomaterials with controlled dimensions and morphology.

Pacchioni & Freund (2013) presented an overview of electronic properties and surface-related defects of MgO. The role of low-coordinated surfaces, defects,

morphological irregularities, and electronic structure on chemical reactivity of MgO for catalytic properties has been discussed. It is highlighted that doping oxides can result in defect engineering, particularly the tendency of transition metal ions in oxide materials to change oxidation state, which may cause non-stoichiometry and defects in the oxide materials.

J. W. Lee & Ko (2014) studied the defect states of TM-doped MgO by the first-principles method. The authors reported a localized (defect) state in Zn-doped MgO film quite close to VBM, which is attributed to the acceptor-like behavior of Zn in MgO thin film that enhances the p-type conductivity of doped MgO by providing holes to the VB. The authors reported an occupied defect level at 0.06 eV above the VB.

Wobbe et al. (2014) undertook a theoretical study of the optical properties of MgO nanoparticles by combining time-dependent DFT and coupled-cluster models. The charge transfer details during the excitation of MgO nanoparticles by light absorption were discussed. From the absorption spectra, it was inferred that the low-coordinated surface sites in MgO nanoparticles, such as 3-coordinated corner sites and 4-coordinated edge sites, have been reported to be involved in the excitation process. In the case of insulating material like MgO, the excitation energy required to create an exciton is highly dependent on the coordination number of O^{2-} ions. MgO NPs with low coordinate states (4C, 3C) have much smaller excitation energy than their bulk counterpart. Thus, to excite an electron in MgO NP, the excitation energy will be much smaller than 7.8 eV. So, the nanoparticles of MgO are synthesized in such a manner that they have more low coordinated states and can be excited at a lower energy.

Zhang et al. (2015) reinforced the role of calcination temperature on the relationship between the surface structure and properties of MgO. The increase in calcination temperature from 400 °C to 1000 °C enhanced the grain boundaries due to a decrease in the size of the particles along with the evolution of crystal structure from mesocrystalline to cubic single crystalline. The electrochemical, catalytic, and reaction selectivity abilities of MgO calcined at different temperatures were modified, illustrating the crucial role of thermal treatments in tailoring the properties of MgO to render it suitable for diverse applications.

Sharma & Jeevanandam (2015) prepared Zn^{2+}-doped MgO nanoparticles from brucite precursors using a sol-gel technique followed by calcination at 500 °C–1000 °C. The optical properties of synthesized samples were studied using DRS and PL spectroscopy. The PL emission bands established the presence of defects in the

synthesized samples. At a calcination temperature of 500 °C, biphase nanocomposites were obtained, but at 1000 °C, single cubic phase doped samples were obtained, and the limit of solubility at 1000 °C in terms of ZnO concentration was proposed to be 28% ZnO in MgO.

Wang et al. (2016) studied the effect of ZnO doping on the electronic structure and optical properties of MgO host material using the theoretical models (DFT, GW, and BSE). The doped samples with rock salt structure have reduced bandgap compared to MgO, which proposed their potential application in optoelectronics as deep UV emitters. It was reported that Zn-doping affected the conduction band edge considerably due to hybridization among outermost s subshells of O, Mg, and Zn rather than the valence band. Moreover, with an increase in the doping concentration of Zn, the decrease in exciton energy and binding energy of the lowermost excited level reduced the light emission properties of bare MgO by Kasha's rule. However, it remains greater than $k_{\beta}T$, hence suitable UV emitters.

Das & Srivasatava (2016) reported electrochemically active nanocomposites of ZnO-MgO synthesized by the co-precipitation method. Compared to pure ZnO electrode, the electrode of mixed metal oxide exhibited a reduction peak in the cyclic voltammetry curve. However, the reflectance of ZnO nanoparticles decreased by ~ 25% with an increase in MgO content in pure ZnO, which is related to an increase in the bandgap of the nanocomposites.

Othman & Matoussi (2016) discussed the effect of MgO-dopant concentration (0-40 %) on morphology and optical properties of ZnO/MgO composites synthesized by solid-state reaction. The band gap was reported to be enhanced (3.29–3.83 eV) in composites due to the Burstein-Moss effect. Moreover, an increase in Urbach tail width was observed with an increase in dopant concentration in this case, which was correlated to an increase in free electron concentration. Thus, an increase in refractive index from 1.33 to 1.9 and energy bandgap in these composites suggest they are suitable for optoelectronic applications.

Xia et al. (2016) studied the temperature-dependent solubility percent of the MgO/ZnO binary system. The solubility of ZnO (wurtzite) in the MgO (rock salt) matrix, computed in this work, varied from 24.6% to 43.5% with an increase in temperature from 1000 °C to 1600 °C. Meanwhile, MgO has been reported to have a considerably smaller solubility in the ZnO Matrix, up to 17%, even at the maximum temperature of 1600 °C of the selected range.

Płóciennik et al. (2016) studied the temperature-dependent linear and non-linear optical properties of pulsed laser-deposited MgO thin film on a quartz substrate. The films deposited at higher substrate temperature (600 °C) are reported to have better quality. The time-resolved PL technique used for the analysis of linear optical properties indicated the MgO thin films to be highly oriented crystalline ones, whereas the third harmonic generation technique revealed feeble temperature dependence of non-linear optical properties. The films with these behaviors are suggested to be suitable platforms for the subsequent overgrowth of other oxides.

Pathak et al. (2016) investigated defect induced photoemission features of sol-gel synthesized MgO compound. Absorption spectroscopy, decay kinetics and TRES characterized multicolour emissions in the visible and NIR regions. DFT theory was employed to correlate the observed photoluminescence with the electronic structure of the MgO compound. A free electron model has been proposed for the observed electronic transitions. Emission spectra were obtained at multiple excitation energies and at temperatures below room temperature.

Cai et al. (2017) prepared silver-doped magnesium oxide nanoparticles through the sol-gel method to improve the efficacy of MgO as an antibacterial remedy. The authors reported a grain growth inhibition effect of Ag-doping, an increase in oxygen vacancies for overall charge neutrality, and a reduction of resistance to electron mobility in a 1% Ag-doped MgO sample that has been associated with the enhancement of antibacterial activity of MgO.

Vasanthi et al. (2017) synthesized 5%, 10% and 15% Zn-doped MgO nanoparticles by sol-gel assisted combustion method and heating finally at 650 °C for WLED applications. Optical band gap of doped samples decreased from 4.6 eV to 3.9 eV with increase in dopant concentration. An increase in number of F-centre defects (F^{o}, $F^{1+}$and F^{2+}) in MgO have been reported with increasing dopant addition. These defects were responsible for the observed PL emissions in the synthesized samples.

Soma & Uchino (2017) reported the synthesis of luminescent Li-doped MgO microcrystals with predominant blue and orange emissions related to an aliovalent doping effect on the bulk and surface electronic structures. The author reported bulk oxygen vacancies and oxygen vacancies at surface sites were responsible for blue and orange emissions, respectively. Thus, Li-doping reduced the bandgap of MgO considerably to give visible emissions.

El-Sayed et al. (2018) discussed the effect of electric fields on structure and migration barriers of canonical defects in MgO using DFT calculations. The canonical defects, including oxygen vacancies and interstitials, in three charge states have been considered in this study. The effect of the applied field is considered in terms of variation in the dipole moment of the system. On application of an electric field, the variation in electronic structures of defects and movement of net excess charge carriers are expected to change the dipole moment of the system. However, it was observed that on applying electric fields, the effective dipole moment change due to net excess charge migration contributed strongly rather than the change in the electronic structure of defects to vary the migration barriers. These effects helped assess the suitability of using MgO in microelectronic devices on the application of external fields.

Obeid et al. (2018) focused mainly on structural and magnetic analysis of the pure and Co-doped MgO nanomaterials synthesized by the co-precipitation method. They reported rock salt cubic single phase below x = 0.12 in $Mg_{(1-x)}Co_{(x)}O$. Doping also resulted in a decrease in the bandgap of MgO. The experimental studies were complemented with theoretical investigation using DFT, which provided insight into various defects, stacking faults, and their variation with doping concentration. Further, their magnetic studies suggested their probable application in spintronics and magnetic data storage.

Ismail et al. (2019) studied the effect of laser fluence on structural and optical properties of nanostructured MgO polycrystalline thin films deposited by PLD at substrate temperature of 100 °C. The MgO film deposited at laser fluence 4.3 J/cm^{-2} was reported be stoichiometric. Further, increase in laser fluence increased the non-stoichiometric nature, particle size, thickness, RMS roughness and band gap of the deposited film.

Hsieh et al. (2019) fabricated Ni/α-Ga_2O_3/Si metal-insulator-semiconductor (MIS) heterojunction diode using the liquid phase deposition method. It was reported in this work that the introduction of an insulating thin film of α-Ga_2O_3 with a wide band gap (~5 eV) has improved the breakdown voltage (~ –166 V) and raised the barrier height of the MIS diode by 0.4 eV as compared to the corresponding MS diode. Hence, an insulating thin film of α-Ga_2O_3 was suggested to have the potential to reduce the inexorable leakage current problem of the MS diode and was suitable for power electronic devices, too.

Misra & Yadav (2019) conducted theoretical studies on various transition metal (TM) doped MgO samples and reported that the small dopant concentration did not affect the insulating properties of MgO. Further, in the case of Zn dopant in MgO, its Zn^{2+} valence state is the most stable charge state as compared to Zn° and Zn^{1+} states because in this charge state, Fermi level lies in the bonding region of the density of states (closer to the VBM). The system with a Fermi level closer to VBM is more stable. The existence of Zn in its most stable valence state is associated with the creation of no additional defect states in the bandgap. Based on the calculation of dopant formation energy for Zn doping in MgO, Debolina reported that Zn prefers interstitial sites in MgO. The author suggested that the ionic radius and oxygen affinity of the transition metal oxide dopant with a similar ionic radius direct the site preference in an ionic metal oxide like MgO.

Sharma et al. (2020) investigated the as-synthesized pure and 5% and 25% Zn-doped MgO nanoparticles prepared by the sol-gel method. Room-temperature PL studies were conducted at an excitation wavelength of 325 nm and reported a red shift in violet emission by all the samples. The violet emission by the samples was assigned to the relaxation of F^{+} centers (defects). These defects were attributed to the surface strains.

Kadri et al. (2020) studied the effect of Li^{+} ion co-doping with Eu^{3+} ion in MgO and reported enhanced photoluminescence lifetimes and reduced defects in Li^{+} and Eu^{3+} co-doped MgO samples. Due to the higher valence state and larger ionic radius of Eu^{3+} ion, its substitution at Mg^{2+} site caused lattice distortion along with charge imbalance in Eu^{3+}-doped MgO. Positron annihilation spectrographic studies revealed that Li^{+} co-doping passivated the defects created by Eu^{3+} with different charge states. Though lower amounts of Li^{+} ion dopant did not affect the octahedral symmetry around Eu^{3+} ion in MgO, its increased amount changed symmetry considerably and created additional O-vacancies.

Hanish et al. (2020) synthesized pure and transition metal (Ni, Cr) doped-MgO nanomaterials using the sol-gel method. The study focussed on investigating the effect of doping of transition metals on the magnetic properties of pure MgO nanoparticles and their probable application in spintronics. It was reported in this work that the room-temperature ferromagnetic nature of pure MgO changed to paramagnetic behavior when doped with Ni and Cr in different ratios. The ferromagnetic ordering in MgO nanomaterials has been attributed to the presence of Mg vacancies, suggesting its

application in spintronic devices. However, doping reduced these defects and hence resulted in paramagnetic ordering.

Divya Rathore and Swati Arora (2020) studied the structural and optical properties of $(ZnO)_x(MgO)_{1-x}$ composite films deposited by electron beam deposition technique on silicon and glass substrates. It was reported that these nanocrystalline thin films had enhanced bandgaps and surface defects in samples with a higher concentration of MgO. Morphological studies showed the porous and rough nature of the films, with a few hexagonal-shaped bigger grains dispersed in nanostructured grains.

Fernandes et al. (2020) presented a review regarding the applications of various nanostructures of MgO. For example, nanoflowers of MgO extracted from rosemary can fight against bacterial infections in agricultural fields, nanosheets of MgO used for strengthening composite materials, and non-toxic and biodegradable MgO NPs for cryosurgery. On suitable tailoring of their properties, MgO NPs have been reported to be efficient biosensors for environmental pollution.

Fazio et al. (2021) presented a review of the chemo-resistive sensing applications of metal oxide-based nanomaterials for detecting toxic gases like H_2, CO, and NO_2. The author highlighted some improvements that can help in realizing a near-ideal gas sensor by optimizing the parameters of the sensing material with respect to sensitivity to humidity, thermal stability, and enhanced selectivity. So, it is crucial to design the material in accordance with the requirements of a particular application.

Munawar et al. (2021) synthesized a novel nanocomposite by mixing three metal oxides- CuO, ZnO, and MgO using co-precipitation method. The synthesized nanocomposite was reported to display efficacy in photocatalytic degradation and bacterial inactivation. The catalyst prepared was witnessed to be reusable efficiently for to five cycles.

Zwijnenburg (2021) conducted a theoretical study to explore the evolution of electronic and optical properties of MgO nanomaterials with variations in particle size. No change in the optical gap was observed due to the strong localization of exciton at the particle's corner atoms, but a change in HOMO/LUMO states with particle size can be assigned to the delocalization of a hole/electron along the edges rather than corner O/Mg atoms respectively. This study also explains the smaller optical gaps in MgO nanoparticles compared to bulk form in terms of highly localized exciton on corner atoms. So, this prototypical ionic oxide (MgO) nanomaterial shows non-quantum mechanical behavior.

Tipaldi & Gabrusenoks (2022) used classical molecular dynamics (MD) to investigate lattice dynamics of solid solutions of MgO and ZnO in variable concentrations. It was reported that in cubic phase doped MgO samples, the increase in concentration of Zn-dopant broadens the density of states (DOS) peak at 350 cm^{-1}, lowering the symmetry and enhancing the disorder of the crystal; however, no vibrational modes corresponding to ZnO were observed. However, due to larger mass of the Zn atom, a red shift in vibrational mode was observed.

Lin et al. (2022) conducted a theoretical study on the electronic and optical properties of Mg-doped ZnO (WZ) and Zn-doped MgO (RS) compounds using density functional theory (DFT). Based on the density of states (DOS), Zn states below CBM were reported to be responsible for the bandgap engineering of these compounds. A red shift in the energy gap with an increase in Zn concentration and a blue shift with an increase in Mg concentration was in accordance with experimental results reported in the literature. Due to different lattice structures, these ZMO compounds exhibit quite different behaviors. However, the concentration of Zn in them predominantly affects the transition states around E_g due to the bonding between Zn and O controlling the edge of CBM.

3. RESEARCH GAP IDENTIFICATION

Through the literature review, it is apparent that magnesium oxide is a suitable insulating interlayer material for reducing the leakage current problem in MIS diode as it is a thermally stable, chemically inert, high *k* (~9.8) material with a wide band gap (~7.8 eV). However, it possesses a large number of intrinsic defects that are detrimental to the device's performance. So, to withstand the continuous scaling process and enhance the performance, it should possess an even higher dielectric constant (k ~ 25–40) and reduced defect density. The reported works conclude that this can be accomplished by doping it with a suitable isovalent metal oxide like ZnO that can modify its microstructure and optical and electronic properties to enhance its dielectric properties while introducing only a minimal amount of strain and lesser defects.

Moreover, most studies on the conductivity of MgO are conducted at temperatures well above 1000 K because the equilibrium concentration of ionic charge carriers that depicts the conduction mechanism could only be attained at high temperatures via the long-range transport of ionic defects. However, it has been mentioned in many works that ionic compounds like MgO may comprise ionic or electronic charge carriers whose

dominance largely depends upon ambient temperature, pressure, and microstructure of the compound. Also, rigorous work has been carried out to investigate the effect of varying oxygen pressure and temperatures (above 800 °C) on the conductivity of MgO. But not much data is available on the conductivity of MgO at low and moderate temperatures. Only a few low-temperature conduction studies have recently been conducted in the range well below 1000 K to investigate dominant conduction carriers of MgO and its doped forms for device applications (P., 2020; Smith et al., 2017). It is reported in these studies that electrons/polarons are the prevailing charge carriers at lower temperatures. However, the temperature dependence of conduction/transport mechanisms in pure and doped-MgO nanomaterials has not been elucidated. Thus, there is a need to explore the temperature-dependent conduction and transport mechanisms of the pure and doped MgO samples using the Arrhenius model over a low and moderate temperature range. To the best of our knowledge, high-temperature dielectric studies of these doped nanomaterials over the temperature range (250–450 °C) for applications as an insulating interlayer in MIS diodes have not been reported earlier. The reported dielectric studies of Zn-doped MgO solid solutions were mainly conducted at room temperature. The effect of dopant concentration on modifying the conductivity mechanism can also have significant implications.

Defects in ionic crystals significantly influence their temperature-dependent conduction behavior. To gain a comprehensive understanding of these materials we will utilize photoluminescent (PL) properties to provide an overview of their inherent defects. Notably, only a few experimental PL investigations on MgO-based ceramic composites have been reported, providing limited insights into reducing prevalent defects and defect density for electronic device applications. Further, reports on the excitation wavelength-dependent photoluminescence to correlate different defect states of these composites with their excitation-emission spectral features that can outline their characteristic role in electronics are scarce.

4. OBJECTIVES OF THE STUDY

Motivated by the above inferences, the present work stands out for its focus on optimizing the synthesis and composition conditions of the MgO/ZnO compound semiconductors. This study aims to synthesize and investigate the unique properties of MgO/ZnO composites and Zn-doped MgO solid solutions, providing new insights into their microstructure, spectroscopic, optical, dielectric and conduction properties. This

research is particularly novel as only a few studies have reported the dominant charge carriers and transport mechanisms in pure and Zn-doped MgO nanomaterials over low to moderate temperature ranges (250–450 °C) and a very limited literature on excitation wavelength-dependent photoluminescence investigations of defects in MgO-based compounds. We intend to fill this research gap by investigating the effect of ZnO doping along with temperature and frequency variation on the dielectric properties and conduction mechanisms of the doped samples. The defects analysis by photoluminescence spectroscopy will help us to know the status of native defects of the host and dopant in the resulting compound semiconductors.

The present research aims to synthesize insulating metal oxide nanostructures with a wide bandgap, high dielectric constant, low defect density, and low loss. The following objectives are set to accomplish the above-stated aim. To synthesize composites of MgO/ZnO using a solid-state reaction method.

- To synthesize ZnO/MgO compound semiconductors using the solid-state reaction method at two different temperatures (500 °C and 1000 °C).
- To investigate the microstructure of the ZnO/MgO compound semiconductors using X-ray diffraction (XRD), scanning electron microscopy (SEM), electron diffraction spectroscopy (EDS), transmission electron microscopy (TEM), and selected area diffraction (SAED).
- To conduct spectroscopic analysis of the ZnO/MgO compound semiconductors using Fourier transform infrared spectroscopy (FTIR), Raman spectroscopy and X-ray photoelectron spectroscopy (XPS).
- To study the optical properties of the ZnO/MgO compound semiconductors using UV-visible and photoluminescent spectroscopy.
- To study the excitation wavelength-dependent photoluminescence of the ZnO/MgO compound semiconductors.
- To study the dielectric and conduction properties of ZnO/MgO compound semiconductors at room temperature and higher temperatures (250–450 °C) using an impedance analyser.

5. PROPOSED METHODOLOGY

5.1 RAW MATERIALS: Pure powders of MgO (97% purity, Sigma Aldrich), ZnO (99.9%, Alfa Aesar), polyvinyl alcohol, potassium bromide, acetone.

5.2 INSTRUMENTS:

- Pestle and mortar
- Hydraulic Press
- Muffle furnace
- X-Ray diffractometer: X'pert Pro PANalytical
- Scanning Electron Microscope: Thermo Scientific FEI Nova SEM 450
- Transmission Electron Microscope: TEM HITACHI (H-7500) 120 kV
- Perkin Elmer SPECTRUM 65 FTIR spectrometer
- RENISHAW MICRO RAMAN spectrometer
- Thermofisher Scientific Nexsa Base Spectrometer
- UV/VIS/NIR LAMBDA-750 and UV/VIS/NIR LAMBDA-1050 spectrometer
- SHIMADZU RF-6000 Spectro fluorophotometer
- WAYNE KERR 6520A and WAYNE KERR 6500B Impedance Analyser

5.3 EXPERIMENTAL PROCEDURE:

- **Synthesis of composites of ZnO/MgO:** Using solid-state reaction method at calcination temperature 500 ℃ for 3 hours.
- **Pelletization:** By adding PVA binder and using a hydraulic press.
- **Sintering:** at 1000 ℃ for 12 hours.
- **Synthesis of solid solutions of ZnO/MgO:** Using solid-state reaction method at calcination temperature 1000 ℃ for 3 hours.
- **Pelletization:** By adding PVA binder and using a hydraulic press.
- **Sintering:** at 1200 ℃ for 12 hours.

5.4 CHARACTERIZATION

The synthesized composites and solid solutions of ZnO/MgO will be characterized for the determination of the phase, size of the grain, structural information, optical bandgap, luminescence, dielectric, and conduction properties of samples. The characterization of sample powders will be done by X-Ray diffractometer (XRD), Scanning Electron Microscope (SEM), Transmission Electron Microscope (TEM), Fourier Transform Infrared (FTIR) spectroscope, RAMAN spectroscope, X-ray photoelectron spectroscope (XPS), UV-Visible spectroscope, and Photoluminescence

spectroscope. Thereafter, dielectric characterization of pellets will be done using Impedance Spectroscopy.

The careful synthesis and characterization of ceramic oxides is essential for their application in any functional device.

5.4.1 MICROSTRUCTURE

5.4.1.1 X-RAY DIFFRACTION (XRD) TECHNIQUE

X-ray diffraction (XRD) techniques are generally employed to envision the structural details such as phase identification, crystallite size and lattice constant of the material. An X-ray diffraction pattern is a plot of the intensity of X-rays scattered at different angles by a sample. The crystal structure determines the position and intensity of the diffraction peaks in an X-ray scattering pattern. Interatomic distances determine the positions of the diffraction peaks. The diffraction peak intensities correspond to the atom types and positions. Diffraction peak widths and shapes are mostly a function of instrument and microstructural parameters. Each diffraction peak is attributed to the scattering from a specific set of parallel planes of atoms. Miller indices (hkl) are used to identify the different planes of atoms. Observed diffraction peaks can be related to planes of atoms to assist in analyzing the atomic structure and microstructure of a sample. Figure 1 illustrates the phenomenon of diffraction of X-rays by crystal planes of a sample.

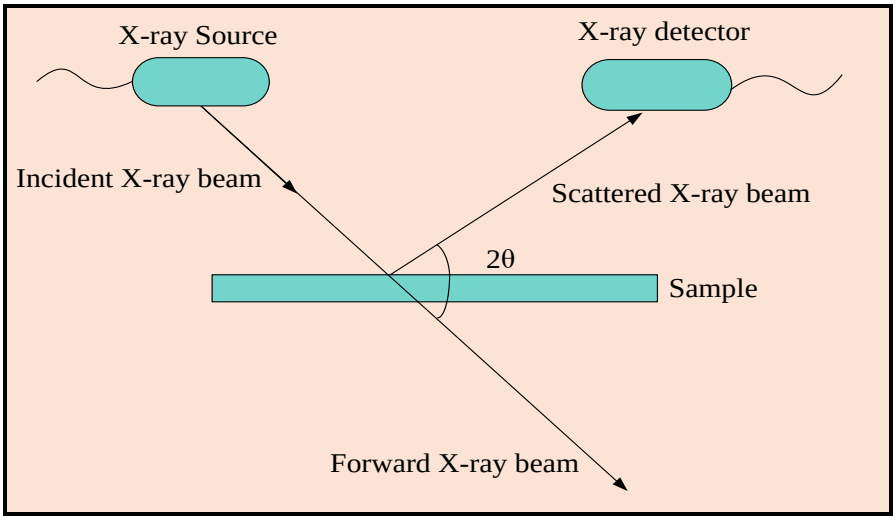

Figure 1 Schematic for diffraction of X-rays by crystal planes

The phase identification of films deposited on substrate can be carried out using X-ray diffraction and corresponding intensity versus 2θ plot. Various diffraction peaks indicate

the crystal structure. The lattice parameters can be estimated from various X-ray diffraction peaks using the relation,

$$\frac{1}{d^2} = \frac{4}{3}\left(\frac{h^2+hk+k^2}{a^2}\right) + \frac{l^2}{c^2} \quad (1)$$

Where, d is the interplaner spacing of atomic planes and (hkl) are the Miller indices, a and c are lattice parameters.

The average crystallite size of particles can be obtained from the full width at half maximum (FWHM) of the diffraction peak using Debye Scherrer equation (Cullity & Stock, 2001).

$$D(2\theta) = \frac{K\lambda}{\beta \cos\theta} \quad (2)$$

Where, $= 0.94$, β is width of diffraction peak measured at half of its maximum intensity in radians, θ is Bragg angle and λ is the wavelength of the X-rays.

5.4.1.2 SCANNING ELECTRON MICROSCOPY (SEM)

Scanning electron microscopy (SEM) is an electron microscopy technique that is capable of achieving a detailed visual image of a particle with high-quality and spatial resolution. SEM is employed to observe the surface phenomena of the materials. The sample is exposed in SEM to the high-energy electron beam and gives information about the topography, morphology, composition, chemistry, orientation of grains, crystallographic information, etc., of a material. Therefore, SEM is a valuable tool for the characterization of materials. Morphology indicates the shape and size, while topography indicates the surface features of an object or "how it looks", its texture, smoothness or roughness. Likewise, composition means elements and compounds that constitute the material, while crystallography means the arrangement of atoms in the materials. SEM, along with XRD, proves to be worthwhile in getting a complete account of the microstructure/morphology of a thin film, as has been reported in many works (Lyman & Dimick, 2012).

5.4.1.3 TRANSMISSION ELECTRON MICROSCOPY

TEM is a crucial technique for applications in materials science and medical science to visualize fundamental structures in a material. It has astonishing analytical capabilities and numerous imaging modes to account for structural and chemical properties (Sciau, 2016). This instrument works on the principle that a highly magnified and resolved

image of the specimen is formed through the interaction of a focused beam of electrons with the specimen. Due to the small de Broglie wavelength of electrons compared to visible light, the TEM image displays a better resolution than that obtained using a light microscope. In 1931, Max Knoll and Ernst Ruska built the earliest transmission electron microscope (TEM), which was reported to have a higher resolution than the light microscope (Fultz & Howe, 2001).

The microscope column consists of an electron gun at the top, which generates either thermionic or field emission electrons. A high-voltage source is connected to the electron gun, which accelerates the electrons to produce a high-energy beam of electrons. Several electromagnetic lenses and apertures are arranged in succession to render a highly focused beam onto the sample. The transmitted electron beam through the sample contains the structural details and is utilized to form the TEM image of the sample. A highly magnified and well-resolved TEM image reaches the detectors. So, when a transmitted beam is utilized to generate a TEM image, then it is called a bright field (BF) image, whereas the image generated by the diffracted beam is called a dark field (DF) image (Shindo & Hiraga, 1998; Smith, 1997). Required vacuum conditions for the effective interaction of electrons with the sample are maintained using a vacuum system included in the column. A computer has been included to control various components in the microscope automatically.

5.4.1.4 FOURIER TRANSFORM INFRARED SPECTROSCOPY

FTIR spectroscopy is an incredibly prevalent technique suitable for solid, liquid and gaseous specimens. It is based on the principle that when IR radiation passes through a sample, it absorbs a part of it, and we get an output corresponding to the transmitted part, which is then converted to the desired spectral information for analysis by a mathematical technique called the Fourier transformation. The FTIR spectrum corresponding to a sample elucidates the absorption of infrared radiations as a function of wavenumber (which is inversely proportional to wavelength). FTIR identifies the presence of organic and inorganic compounds in the sample from the corresponding molecular fingerprints, as no two dissimilar samples can evince similar FTIR spectra due to the unique arrangement of atoms in each sample. The molecular fingerprint lies in the region below wavenumber 1000 cm^{-1} in the FTIR spectrum. The IR energy absorbed by the molecules is characteristic of the type of bonding and the nature of atoms bonded that cause excitation of vibrational modes. The covalent bonds between the atoms are like

springs which can undergo stretching, bending, rotating and scissoring kind of vibratory motions on the absorption of IR. The mid-IR region (400–4000) cm^{-1} stimulates the fundamental vibratory modes in the samples. The intensity of the absorption bands is also related to the dipole moment of the irradiated sample. No variation in dipole moment renders the molecules to be IR inactive.

FTIR spectrometer is a versatile instrument for obtaining microstructural elucidation of samples of different states, forms and sizes, as it has interchangeable accessories for solid, liquid and gaseous samples. This technique performs better than a conventional IR spectrometer regarding scanning speed, resolving power, and accuracy. However, in some instruments, IR transparent KBr powder is mixed with a small amount of sample for carrying out analysis that has constraints regarding time and reproducibility. Modern advanced FTIR instruments have been designed to address all the limitations of existing FTIR spectrometers.

5.4.1.5 RAMAN SPECTROSCOPY

Raman Spectroscopy is a non-destructive versatile analysis technique which provides detailed information about the vibrational modes, chemical structure, phase and crystallinity of a sample under study (solid, liquid or gas) (Gouadec & Colomban, 2007; Rostron et al., 2016). Actually the Raman spectrum depicts the energies corresponding to vibrational and rotational modes which in turn are the manifestations of the composition, symmetry, type of bonding and crystallinity of a sample. It is based upon the principle of interaction of light radiation with the chemical bonds within the sample. In this molecular spectroscopy, when a monochromatic beam interacts with the sample, it gets scattered into two types of light via two different scattering modes:

(i) **Rayleigh (elastic) scattering**: A significant part of the incident light suffers elastic scattering, and thus, the scattered light in this process has the same frequency as that of incident light. This phenomenon is known as Rayleigh scattering.

(ii) **Raman (inelastic) scattering**: A smaller part of incident light undergoes inelastic scattering and has a frequency either greater or lesser than the incoming light. So if the frequency of scattered light is smaller than incident light, then this is called Stoke's scattering, and if it is greater than the frequency of incident light, then this phenomenon is called Anti-Stoke's scattering. Accordingly, the spectral lines in the spectra are named Stoke's lines if the electrons excited from

the ground state return to some state above the ground state, thus emitting a lower energy photon, and Anti-Stoke's lines if the electrons excited from some state above the ground state returns to ground state thus emitting a higher energy photon.

The change in frequency of the scattered light with respect to that of the incident frequency, also called Raman shift (Δν) in Raman spectroscopy, is given by equation (3)

$$\Delta\nu = \nu_o \pm \nu_m \quad (3)$$

Where, spectral lines with frequencies $\nu_o - \nu_m$ and $\nu_o + \nu_m$ are called the Stokes and anti-Stokes lines respectively (Ferraro et al., 2003).

To measure Raman shift (Δν), an intense, collimated and monochromatic excitation source, i.e. a laser, is employed in Raman spectroscopy, which enables the measurement of even a relatively small change in frequency. The wavelength of the excitation source should be optimized to get a better differential scattering cross-section, which is inversely proportional to the fourth power of the wavelength of the laser, with no intrusion with the weaker Raman scattered light. Scattered light is passed through spectrometers to isolate the smaller Raman scattered component from the major Rayleigh scattered part.

5.4.1.6 X-RAY PHOTOELECTRON SPECTROSCOPY

X-ray photoelectron spectroscopy (XPS) is a surface sensitive (up to ~ 1 to 10 nm), and non-destructive technique to determine the elemental composition and the chemical bonding of the sample. The spectroscope has three basic components: an X-ray source, an electron analyzer, and a detector. XPS spectrum of a sample is obtained under ultra-high vacuum conditions as mean free path of ejected electrons is inversely proportional to the ambient pressure. X-ray photons incident onto a sample are absorbed by the electrons of its surface atoms and are ejected from the sample with a definite kinetic energy. The kinetic energy of emitted electrons is measured by the detector in the spectrometer. The binding energy of electrons can be obtained using following equation (4)

$$E_B = E_{h\nu} - (E_k + \phi) \quad (4)$$

Where, E_B is binding energy of an electron, $E_{h\nu}$ is the energy of X-ray photon, E_k is the kinetic energy of the ejected electron and ϕ is the work function. A plot of binding energy of the emitted electrons versus relative number of electrons ejected comprises a number of peaks corresponding to the electrons emitted from particular states. The shape and position of the peaks in the XPS spectrum reveal the oxidation states, nature of hybridization and partial charges on the elements. This surface technique has a limitation of displaying relatively lower concentrations of existing elements due to the contamination of the top surface by noticeable amount of environmental carbon and oxygen.

5.4.2 OPTICAL CHARACTERIZATION

One of the fundamental properties of metal oxides includes the optical properties that can be studied by obtaining absorption and photo-luminescent spectra of these materials. Absorption of light photons causes excitations. In the case of nanostructured metal oxides, a dramatic variation in the electronic structure of the material takes place, due to which absorption spectra change significantly, suffering red/blue shifts, which are highly size and composition-dependent in the case of composites or doped metal oxides. The dopant concentration and dopant site in the host lattice prompt diversity in the electronic structure and optical response of these composites. A red or blue shift of the excitonic peak observed in the absorption spectra directly relates to the bandgap modification. However, the anisotropy induced by the location of dopant ions in the host lattice in the composites may also result in a spectral shift of these excitonic peaks. The interband transitions in these composites are closely related to the abundance of donor levels below the CBM, which is a function of dopant concentration (Lin et al., 2022). The two major optical properties which play a critical role in defect analysis, bandgap and luminescence of the metal oxide nanostructures, are discussed below.

5.4.2.1 UV-VISIBLE SPECTROSCOPY

UV-Vis spectroscopy is an analytical technique that measures the amount of discrete wavelengths of UV or visible light absorbed by or transmitted through a sample compared to a reference sample. The absorption spectra of the ionic metal oxides generally exhibit a sharp absorption peak in the ultraviolet region, which characterizes the optical bandgap. The band-to-band transition of bulk metal oxides can be modified by obtaining nanostructures and doping metal oxides (Pacchioni & Freund, 2013). The presence of low-coordinated sites in nanostructured metal oxides like 5-coordinated terrace (5C), 4-coordinated (4C) edge, or 3-coordinated (3C) corner sites can drastically

change its bandgap. This may be assigned to the lesser stabilization of 2p levels of O^{2-} ions on the low-coordinated sites (3C or 4C), which result in the introduction of additional energy states in their bandgap of the metal oxide (Wobbe et al., 2014).

The bandgap energy E_g of metal oxide nanostructures can be determined by plotting the Tauc plot, which considers the dependence of the absorption coefficient on the photon energy according to the following equation

$$\alpha h\nu = A(h\nu - E_g)^n \quad (5)$$

where A is a constant and n takes a value of 1/2 or 2 depending on whether the sample has a direct or indirect bandgap. For the direct bandgap materials, n=1/2 and for the indirect bandgap materials, n=2. So equation (5) for the direct bandgap metal oxides becomes (Das & Srivasatava, 2016)

$$\alpha h\nu = A(h\nu - E_g)^{\frac{1}{2}} \quad (6)$$

From the plot of $(\alpha h\nu)^2$ vs E_g (photon energy), the energy bandgap of the samples has been calculated from the intercept obtained by extrapolating the linear part of $(\alpha h\nu)^2$ vs E_g at the energy axis.

A considerable change in the bandgap of composites of binary metal oxides has been reported in many works. The increase or decrease in bandgap depends upon various factors, such as the nature of the host and dopant, synthesis conditions, size of the nanostructures, and concentration of the dopant (Kant et al., 2022; Priyadarshini et al., 2021). The reduction in energy band gap may be assigned to the introduction of donor/acceptor energy levels below/above the conduction band minima (CBM)/valence band minima (VBM) in the composites (Lin et al., 2022; Vasanthi et al., 2017; Wang et al., 2016).

5.4.2.2 PHOTOLUMINESCENCE SPECTROSCOPY

Photoluminescence is the emission of light from a material on the absorption of electromagnetic radiation photons. The emission/excitation spectra obtained by this technique account not only for the luminescent properties and bandgap but also precisely estimate the defects, disorder and impurity in the bulk as well as on the surface/interface of a material. This technique is particularly suitable for direct wide bandgap materials. In nanocrystalline materials, luminescence is associated with low-coordinated surface states (Kadri et al., 2020; Soma & Uchino, 2017; Sternig et al., 2012).

Thus, in this work, the PL technique has been utilized to study the luminescent properties of nanocrystalline direct wide bandgap pure and doped metal oxides to

explore various surface defects that might have been created in the synthesized nanostructures that are responsible for various emissions. This technique is advantageous due to its proficiency and non-destructive nature. It involves three processes: excitation, non-radiative transitions and radiative transitions. The luminescence can be intrinsic or extrinsic depending upon the contribution to the electronic transitions by intrinsic or extrinsic defect states, created intentionally by adding impurity in a material. Most of the practical applications and research focus on the investigation of extrinsic luminescence in materials, which allows tuning the desired luminescent properties by controlling various synthesis and composition-related parameters (Kumar et al., 2011; Selvam et al., 2011). Adding impurities enhances luminescence and can even introduce luminescent properties in an otherwise non-luminescent ceramic metal oxide. The ceramic oxides generally display UV excitonic luminescence and are transparent to visible regions, but the addition of TM oxides is reported to introduce defect levels in the bandgap of these host oxides, which cause visible light emissions (Abhijith et al., 2020; Othman & Matoussi, 2016; Vasanthi et al., 2017). Luminescence, owing to band-to-band transition, takes place when the relaxation of an electron from the conduction band leads to recombination with a hole in the valence band.

Many theoretical studies have made a successful attempt to present surface structural features of defects in MgO and ZnO (Mulroue & Duffy, 2011; Wang et al., 2016), but a perfect correlation between modulated surface features and corresponding electronic properties in Zn-doped MgO compounds is still not very clear. In nanoscale dimensions, these oxide compounds have low-coordinated surface ions that play a very crucial role in surface properties such as charge transfer on photon irradiation, photocatalytic response and leakage current at insulating oxide-semiconductor interface in electronic devices (Sushko et al., 2002). Knowledge concerning the excitation of a definite surface location on irradiation with a specific photon excitation wavelength is necessary for understanding the modulated surface features and transport mechanisms via electronic properties in the doped samples. The dependence of excitation energies on coordination no. of surface O-ions in MgO has been discussed in many works. The excited states in CB and surface terrace sites can transfer charge to low-coordinated sites, causing luminescence. In powdered sample of MgO numerous edge and corner sites are occupied by cationic or anionic ions. Sushko et al. (2002) calculated ionization energies and electron affinities of different defect sites, depicting their charge trapping probabilities to cause localized charge states. These may help acquire information regarding excitation

of a specific surface site at a particular photon excitation wavelength and transport mechanisms via electronic properties in the doped samples.

Sushko et al. (2002) demonstrated through theoretical study that holes preferably localize at 3C (corner) O-ions. In contrast, electrons rather localize at 3C Mg-ions even if they are delocalized at terrace and edges due to their lower energies at 3C sites. The authors also calculated the optical excitation energies of defects in these low-coordinated sites. Misra & Yadav (2019) mentioned that if the ionic radii of the dopant and host are nearly the same, then the relative site preference of the dopant is determined by electron affinity (EA) of the cationic/anionic sites. The deep-level traps, which include O^{2-} ions (at terrace, edge and corner), have EA of more than 2 eV, whereas shallow traps have EA ~ 1–2 eV. Though bandgap is a standard parameter for bulk insulating oxides, in nanostructured samples, some additional parameters such as ionization potential and electron affinity are required to characterize their surface features (Pacchioni, 2001).

5.4.3 DIELECTRIC PROPERTIES

Recently, researchers have focused on investigating the dielectric properties, electric modulus, and AC conductivity of these insulating materials over a range of frequency, bias, and temperature to gain a deep insight into the significance of these properties for the power consumption, dielectric relaxation, and high-frequency operation of the device.

5.4.3.1 DIELECTRIC PERMITTIVITY (ε*)

When a time-varying voltage is applied to a dielectric material, then a time-dependent field $E(t)$ is established, and polarization of the material takes place given by the formula

$$\mathrm{P}(\mathrm{t}) = \varepsilon_o(\varepsilon_r - 1)E(t) \qquad (7)$$

Polarization P (t) also becomes time-dependent, and a part of it exactly follows the variations of E(t), which is associated with the storage of energy, whereas the other part of it is associated with energy dissipation in the form of heat. It means some of the induced charges in the dielectric will move in phase with the applied field and contribute to the permittivity(ε') while the rest of the induced charges will oscillate out of phase with the applied field with a phase shift angle ‘δ’, resulting in energy dissipation and contribute to the permittivity (ε''). Therefore, the absolute permittivity of the material is a complex quantity and comprises of real and imaginary parts

$$\varepsilon^* = \varepsilon' - \varepsilon'' \quad (8)$$

Where, the real part of the permittivity accounts for the energy storage of the material (dielectric constant), and the imaginary part accounts for the dielectric loss in the form of heat.

Dielectric dispersion takes care of the frequency dependence of the permittivity of dielectric material. Permittivity decreases with increasing frequency, and the decrease is steep at a characteristic frequency, i.e. relaxation frequency where dielectric loss is maximum due to dielectric relaxation. The plot of permittivity versus frequency at the characteristic frequency peak appears corresponding to the dielectric loss. At high frequencies, there is a contribution due to electronic polarization only and dielectric relaxation (loss) decreases. However, at very high frequencies, there is no contribution due to the interface and dipole polarizations, as the trap charges cannot follow the high-frequency alternating signal, so the value of the dielectric constant is quite small. Resonances are observed at higher frequencies. So, dielectric relaxation is a low-frequency phenomenon.

5.4.3.2 DIELECTRIC CONSTANT (ε_r)

It is also called relative permittivity of a material that accounts for the energy stored in the material whenever a voltage is applied on it. It can also be defined in terms of ratio of the capacitance of a capacitor with dielectric material to its capacitance with vacuum between its two plates.

$$\varepsilon_r = \frac{\varepsilon}{\varepsilon_o} \quad (9)$$

Where, ε_r is relative permittivity, ε is complex frequency dependent absolute permittivity of material or permittivity of medium and ε_o is permittivity of free space

The increase observed in values with temperature is due to the contribution of the charge carriers to the polarization. At low temperatures, polarization is weak due to inability of the dipoles to rotate fast enough; therefore, they oscillate behind the field. The increase in temperature provides sufficient thermal excitation energy to the bound charge carriers, which enhances the polarization, leading to the increase in the dielectric constant.

5.4.3.3 DIELECTRIC LOSS TANGENT (tan δ)

It is the measure of energy loss caused in a dielectric material in the form of heat whenever a variable electric field is applied.

$$\tan\delta = \frac{\varepsilon''}{\varepsilon'} \quad (10)$$

Where, δ is the loss factor i.e. the phase difference between the induced current in the material and applied field and $\tan\delta$ is related to real and imaginary dielectric constant.

There are several mechanisms by which a dielectric material can dissipate energy gained from an applied electric field, such as dipole relaxation, hopping of charges, and damping of molecular and electronic vibrations. These processes are effective over a limited frequency range, and in most cases, at a particular frequency, just one of the above-mentioned dissipative processes is effective. So, $\tan\delta$ measures the power dissipated.

5.4.3.4 AC CONDUCTIVITY

The real and imaginary parts of complex conductivity $\sigma^* = \sigma' - \sigma''$ attributed to hopping of charge carriers are given by equations (11) and (12) representing Jonscher's Power law and the high-frequency linear behavior due to the ε_∞ contribution, respectively (Seeger et al., 1999; Sichelschmidt et al., 2001).

$$\sigma'(\omega) = \sigma_{dc} + A\omega^s \quad (11)$$

$$\sigma''(\omega) = \tan\left(\frac{s\pi}{2}\right)\sigma_0 A\omega^s + \varepsilon_\infty\varepsilon_o \quad (12)$$

Where, σ_{dc} is DC conductivity, A is a constant, s is frequency coefficient ($0< s<1$), ε_o and ε_∞ represent static and dynamic dielectric constant. Frequency coefficient (s) is a significant factor that evinces the degree of interaction between the charge carriers and the lattice. Recently, the frequency coefficient has been recurrently used to illustrate the conduction mechanisms and the prevailing dominant carriers in diverse materials.

Seeger et al. (1999) reported high-frequency linear behavior (with frequency coefficient s ~1) in their work. They suggested that the real part of conductivity (σ') had a contribution from second universality (SU) in addition to universal dielectric response (UDR). Super-linear dependence of conductivity on frequency with frequency exponent >1 has also been reported in some works that had been attributed to re-orientational hopping (Husain et al., 2013; Sichelschmidt et al., 2001). Moreover, the imaginary part of conductivity σ'' also explains the high-frequency linear behavior, observed in our samples due to the contribution from static dielectric constant (ε_∞).

The DC conductivity of samples can be expressed conventionally in terms of activation energy E_a given by Arrhenius equation (13)

$$\sigma(T) = \sigma_o \exp(E_a/k_\beta T) \quad (13)$$

Where, σ_o is specific conductivity, k_β is Boltzmann constant and T is absolute temperature. The activation energy E_a is the sum of formation energies and migration energies of dominant charge carriers in the lattice.

At low temperatures (extrinsic region), formation energies do not contribute to the activation energy due to non-attainment of equilibrium. Hence, only the migration energies of charge carriers contribute to Arrhenius energy (Davies, 1963; Kao, 2004; Smith et al., 2017). Smith et al. (2017) reported migration energies of hole polaron (p^+) in MgO to be of the order (0.11–0.25) eV. They suggested small migration energy of hole polaron due to its high mobility μ (6×10^{-3} cm^2 /Vs). The creation of hole polaron in the MgO lattice has been supported by changes in bond length and density of states (DOS) calculations, which further introduced a trap state above the Valence Band Maximum (VBM) by removing electrons from π* orbital of oxygen.

Almost flat curves in $\sigma_{ac}(\omega)$ versus temperature plots indicate the less significant variation of AC conductivity with temperature, which designates the typical dielectric behavior. However, slight variations with temperature can occur due to the thermal fluctuations in the lattice, which increase the probability of escaping carriers from trap states to cause conductivity.

Thermally activated charge carriers follow the Arrhenius relation, which indicates an exponential rise of their conductivity with temperature according to equation (13). The Arrhenius equation relates to band conductivity, which is a high-temperature phenomenon for insulating ionic oxides. At lower temperatures, charge carriers remain localized as they do not have sufficient thermal energy to delocalize them.

6. THESIS OUTLINE

Chapter 1 (Introduction): This chapter will provide a comprehensive overview of the historical background, types of metal oxides, and various strategies for engineering metal oxides. It will delve into the diverse applications and properties of nanostructured metal oxides. The focus of this study on the structural, optical, and luminescent features, as well as dielectric and conduction properties of metal oxide nanostructures, will be highlighted. An account of crystal structure, defects, and prevalent conduction mechanisms of the metal oxides chosen in the present study will be presented. The

chapter will conclude by outlining the aims and objectives of the study, emphasizing its novelty in the field of metal oxide nanostructures.

Chapter 2 (Literature Review): This chapter will deal with the intense literature survey regarding the synthesis and properties of the compounds related to chosen materials (MgO and ZnO). The focus will be mainly on the defects, optical, dielectric, and conduction properties of pure and doped nanomaterials. Specifically, the research gap and motivation for the present work, which is to further explore the properties of these materials and contribute to the existing knowledge, will be identified.

Chapter 3 (Materials and Methods): This chapter will focus on the detailed synthesis procedure for the pure and doped-MgO nanostructures, including the specific materials used and the steps involved. It will also cover the fundamentals of various experimental and characterization techniques to be used in the present research, such as XRD, FTIR, SEM, TEM, Raman, XPS, UV-Vis spectroscopy, PL spectroscopy, and Impedance Analyzer, providing a comprehensive understanding of the experimental process and reproducibility of the results.

Chapter 4 (Result and Discussion): This chapter will cover a detailed discussion of the results of the present research regarding the structural analysis (XRD, FTIR, Raman, XPS, SEM and TEM), Optical analysis (UV-Vis spectrometry and PL spectrometry) and dielectric analysis (Impedance Analyser) of the synthesized pure MgO, ZnO/MgO composites and Zn-doped MgO nanoparticles. The effect of varying dopant (ZnO) concentration on the structure, morphology and optical bandgap of MgO nanoparticles will be presented. The room temperature dielectric and luminescent properties of the synthesized samples and the effect of temperature variation on the dielectric properties and conduction mechanisms of these Zn-doped MgO samples will be discussed. Further, multiple-excitation wavelengths will be employed to identify the defects corresponding to different low-coordinated sites in the samples, providing a comprehensive understanding of the materials' properties.

Chapter 5 (Conclusion): This chapter will summarize the study according to the objectives and include conclusions.

7. RESEARCH PLAN SCHEDULE

Research activity, extensive literature survey/design of work, attending workshops and international conferences organized on relevant fields, research gap identification and development of methodology, preparation and characterization of the samples, manuscript preparation for publications, and thesis writing.

8. REFERENCES

1 Abhijith, A.R., Srivastava, A.K., Srivastava, A. (2020) Synthesis and Characterization of Magnesium Doped ZnO Using Chemical Route. *Journal of Physics: Conference Series*, 1531, 012005. Available from: https://doi.org/10.1088/1742-6596/1531/1/012005

2 Adhlakha, N., Yadav, K.L., Kumar, A., Patel, P.K., Rani, J., Rawat, M. (2012) Structural, optical and magnetic study of (1-x) ZnO-xMgO composites prepared through solid state reaction method. *Physica B: Condensed Matter*, 407(17), 3427–3433. Available from: https://doi.org/10.1016/j.physb.2012.04.052

3 Athar, T., Hakeem, A., & Ahmed, W. (2012) Synthesis of MgO nanopowder via non aqueous sol-gel method. *Advanced Science Letters*, *7*, 27–29. Available from: https://doi.org/10.1166/asl.2012.2190

4 Balamurugan, B. & Mehta, B.R. (2001) Optical and structural properties of nanocrystalline copper oxide thin films prepared by activated reactive evaporation. *Thin Solid Films*, 396(1-2), 90–96. Available from: https://doi.org/10.1016/S0040-6090(01)01216-0

5 Baranov, A.N., Kapitanova, O.O., Panin, G.N. & Kang, T. V. (2008) ZnO/MgO nanocomposites generated from alcoholic solutions. *Russian Journal of Inorganic Chemistry*, 53, 1366–1370. Available from: https://doi.org/10.1134/S0036023608090040

6 Cai, Y., Wu, D., Zhu, X., Wang, W., Tan, F., Chen, J., Qiao, X., Qiu, X. (2017) Sol-gel preparation of Ag-doped MgO nanoparticles with high efficiency for bacterial inactivation. *Ceramic International*, 43, 1066–1072. https://doi.org/10.1016/j.ceramint.2016.10.041

7 Chawla, S., Jayanthi, K., Chander, H., Haranath, D., Halder, S.K. & Kar, M. (2008) Synthesis and optical properties of ZnO/MgO nanocomposite. *Journal of Alloys and Compounds*, 459(1-2), 457–460. Available from: https://doi.org/10.1016/j.jallcom.2007.04.303

8 Chen, X.Y., Wong, K.H., Mak, C.L., Yin, X.B., Wang, M., Liu, J.M. & Liu, Z.G. (2002) Selective growth of (100)-, (110)-, and (111)-oriented MgO films on Si (100) by pulsed laser deposition. *Journal of Applied Physics*, 91(9), 5728–5734. Available from: https://doi.org/10.1063/1.1461059

9 Chinthala, M., Balakrishnan, A., Venkataraman, P., Gowtham, V. & Polagani, R. (2021) Synthesis and applications of nano-MgO and composites for medicine, energy, and environmental remediation: a review. *Environmental Chemistry Letters*, 19, 4415–4454. Available from: https://doi.org/10.1007/s10311-021-01299-4

10 Cullity, B. D. & Stock, S. R. (2001) *Elements of X-ray Diffraction*. 3rd Edition, Prentice Hall.

11 Das, S. & Srivasatava, V.C. (2016) Synthesis and characterization of ZnO-MgO nanocomposite by co-precipitation method. *Smart Science*, 4(4), 190–195. Available from: https://doi.org/10.1080/23080477.2016.1260425

12 Davies, M.O. (1963) Transport phenomena in pure and doped magnesium oxide. *The Journal of Chemical Physics*, 38, 2047–2055. Available from: https://doi.org/10.1063/1.1733932

13 Desai, P., Darji, V., Deshpande, M.P., Chaki, S.H., Solanki, P.S., Shah, N.A. & Hirpara, B. (2023) Synthesis and dielectric studies of Ni doped MgO nanostructure. *Inorganic and Nano-Metal Chemistry*, 1-13. Available from: https://doi.org/10.1080/24701556.2023.2260373

14 D'Souza, L. & Richards, R. (2007) 3-Synthesis of Metal-Oxide Nanoparticles: Liquid-Solid Transformations. In: Rodríguez, J.A. & Fernández-Garcia, M. (Eds.) *Synthesis, Properties, and Applications of Oxide Nanomaterials*. John Wiley & Sons, pp. 81 – 117. Available from: https://doi.org/10.1002/9780470108970.ch3

15 El-Sayed, A.M., Watkins, M.B., Grasser, T. & Shluger, A.L. (2018) Effect of electric field on migration of defects in oxides: Vacancies and interstitials in bulk MgO. *Physical Review B*, 98, 064102. Available from: https://doi.org/10.1103/PhysRevB.98.064102

16 Fazio, E., Spadaro, S., Corsaro, C., Neri, Giulia, Leonardi, S.G., Neri, F., Lavanya, N., Sekar, C., Donato, N. & Neri, G. (2021) Metal-oxide based nanomaterials: Synthesis, characterization and their applications in electrical and electrochemical sensors. *Sensors*, 21(7), 2494. Available from: https://doi.org/10.3390/s21072494

17 Fernandes, M., RB Singh, K., Sarkar, T., Singh, P. & Pratap Singh, R. (2020) Recent Applications of Magnesium Oxide (MgO) Nanoparticles in various domains.

Advanced Materials Letters, 11(8), 1–10. Available from: https://doi.org/10.5185/amlett.2020.081543

18 Ferraro, J. R., Nakamoto, K. & Brown, C. W. (2003) 2-Instrumentation and Experimental Techniques. In: *Introductory Raman Spectroscopy*. 2nd edition, Academic Press, pp. 95–146. Available from: https://doi.org/10.1016/B978-012254105-6/50005-6

19 Fultz, B. & Howe, J. M. (2001) 7-Diffraction Contrast in TEM Images. In: B. Fultz & J. M. Howe (Eds.), *Transmission Electron Microscopy and Diffractometry of Materials*. Springer Berlin Heidelberg, pp. 339–422. Available from: https://doi.org/10.1007/978-3-662-04516-9_7

20 Gouadec, G. & Colomban, P. (2007) Raman Spectroscopy of nanomaterials: How spectra relate to disorder, particle size and mechanical properties. In: *Progress in Crystal Growth and Characterization of Materials*, 53(1) pp. 1–56. https://doi.org/10.1016/j.pcrysgrow.2007.01.001

21 Hafef, O., Othman, Z.J., Megdich, M. & Matoussi, A. (2017) Conduction mechanism and dielectric properties of ZnO/MgO solid composites. *Applied Physics A: Materials Science and Processing*, 123, 95. Available from: https://doi.org/10.1007/s00339-016-0721-4

22 Hanish, H.H., Edrees, S.J. & Shukur, M.M. (2020) The effect of transition metals incorporation on the structural and magnetic properties of magnesium oxide nanoparticles. *International Journal of Engineering, Transactions A: Basics* 33(4), 647–656. Available from: https://doi.org/10.5829/IJE.2020.33.04A.16

23 Hsieh, Y.S., Li, C.Y., Lin, C.M., Wang, N.F., Li, J. V. & Houng, M.P. (2019) Investigation of metal-insulator-semiconductor diode with alpha-Ga_2O_3 insulating layer by liquid phase deposition. *Thin Solid Films* 685, 414–419. Available from: https://doi.org/10.1016/j.tsf.2019.06.044

24 Husain, S., Bhat, I., Khan, W. & Al-Khataby, L. (2013) Structural and dielectric properties of $La_{0.8}Te_{0.2}MnO_3$. *Solid State Communications* 157, 29–33. Available from: https://doi.org/10.1016/j.ssc.2012.12.019

25 Ismail, R.A., Mousa, A.M. & Shaker, S.S. (2019) Pulsed laser deposition of nanostructured MgO film: Effect of laser fluence on the structural and optical properties. *Materials Research Express*, 6, 075007. Available from: https://doi.org/10.1088/2053-1591/ab1208

26 Kadri, G.B., Das, D., Gupta, S.K. & Sudarshan, K. (2020) Influence of Li^{+} co-doping on the luminescence of MgO: Eu^{3+} nanocrystals: Probing asymmetry, energy transfer and defects. *Solid State Sci*ences, 105, 106286. Available from: https://doi.org/10.1016/j.solidstatesciences.2020.106286

27 Kant, R., Agarwal, Y.K., Kumar, K., Bansal, S. & Kaul, S. (2022) Superior dielectric behaviour and band gap tuning of Zn doped MgO nanoparticles. *Materials Technology*, 37, 3017–3024. Available from: https://doi.org/10.1080/10667857.2022.2110795

28 Kao, K.C. (2004) 7-Electrical Conduction and Photoconduction: With Emphasis on Physical Concepts of Electronic Processes. In: *Dielectric Phenomena in Solids*. Academic Press, pp. 381-514. Available from: https://doi.org/10.1016/b978-012396561-5/50017-7

29 Kaur, D., Bharti, A., Sharma, T. & Madhu, C. (2021) Dielectric Properties of ZnO-Based Nanocomposites and Their Potential Applications. *International Journal of Optics*, 2021, 9950202. Available from: https://doi.org/10.1155/2021/9950202

30 Kumar, A., Thota, S., Varma, S. & Kumar, J. (2011) Sol-gel synthesis of highly luminescent magnesium oxide nanocrystallites. *Journal of Luminescence*, 131, 640–648. Available from: https://doi.org/10.1016/j.jlumin.2010.11.008

31 Kumar, S., Singh, V. & Tanwar, A. (2016) Structural, morphological, optical and photocatalytic properties of Ag-doped ZnO nanoparticles. *Journal of Materials Science: Materials in Electronics*, *27*(2), 2166–2173. Available from: https://doi.org/10.1007/s10854-015-4227-1

32 Kwo, J., Hong, M., Busch, B., Muller, D.A., Chabal, Y.J., Kortan, A.R., Mannaerts, J.P., Yang, B., Ye, P., Gossmann, H., Sergent, A.M., Ng, K.K., Bude, J., Schulte, W.H., Garfunkel, E. & Gustafsson, T. (2003) Advances in high κ gate dielectrics for Si and III–V semiconductors. *Journal of Crystal Growth*, 251, 645–650. Available from: https://doi.org/10.1016/S0022-0248(02)02192-9

33 Lee, J.W. & Ko, J.H. (2014) Defect states of transition metal-doped MgO for secondary electron emission of plasma display panel. *Journal of Information Display*, 15, 157–161. Available from: https://doi.org/10.1080/15980316.2014.955140

34 Lee, S.H., Jeon, Y.P., Lee, E.J., Lee, Y.J., Cho, T.W., Kim, G.H., Ko, E., Park, J.S., Moon, Y. Il, Park, S.Y. & Yoo, Y.J. (2023) Enhanced dielectric properties of Be-

doped magnesium oxide nanopowder. *AIP Advances*, 13, 015007. Available from: https://doi.org/10.1063/5.0130595

35 Lin, Y.P., Piskunov, S., Trinkler, L., Ming-Chi Chou, M. & Chang, L. (2022) Electronic and Optical Properties of Rocksalt Mg1−xZnxO and Wurtzite Zn1−xMgxO with Varied Concentrations of Magnesium and Zinc. *Materials*, 15(21), 7689. Available from: https://doi.org/10.3390/ma15217689

36 Lu, H.-L. & Zhang, D.W. (2012) 2-Issues in High-k Gate Dielectrics and its Stack Interfaces. In: He, G. & Sun, Z. (Eds.), *High-k Gate Dielectrics for CMOS Technology*. Wiley, pp. 31-59. Available from: https://doi.org/10.1002/9783527646340.ch2

37 Lyman, C. & Dimick, P. (2012) Advanced STEM Microanalysis of Bimetallic Nanoparticle Catalysts. *AIP Conference Proceedings*, *1437*, 85–88. https://doi.org/10.1063/1.3703348

38 Misra, D. & Yadav, S.K. (2019) Prediction of Site Preference of Implanted Transition Metal Dopants in Rock-salt Oxides. *Science Reporter*, 9, 12593. Available from: https://doi.org/10.1038/s41598-019-49011-5

39 Mulroue, J. & Duffy, D.M. (2011) An ab initio study of the effect of charge localization on oxygen defect formation and migration energies in magnesium oxide. In: *Proceedings of the Royal Society A: Mathematical, Physical and Engineering Sciences*. pp. 2054–2065. Available from: https://doi.org/10.1098/rspa.2010.0517

40 Munawar, T., Mukhtar, F., Yasmeen, S., Naveed-ur-Rehman, M., Nadeem, M.S., Riaz, M., Mansoor, M. & Iqbal, F. (2021) Sunlight-induced photocatalytic degradation of various dyes and bacterial inactivation using CuO–MgO–ZnO nanocomposite. *Environmental Science and Pollution Research*, 28, 42243–42260. Available from: https://doi.org/10.1007/s11356-021-13572-8

41 Narayan, J., Sharma, A. K., Kvit, A., Jin, C., Muth, J. F., & Holland, O. W. (2001) Novel cubic ZnxMg1-xO epitaxial heterostructures on Si (100) substrates. *Solid State Communications*, *121*(1), 9–13. Available from: https://doi.org/10.1016/S0038-1098(01)00431-8

42 Obeid, M.M., Edrees, S.J. & Shukur, M.M. (2018) Synthesis and characterization of pure and cobalt doped magnesium oxide nanoparticles: Insight from experimental and theoretical investigation. *Superlattices and Microstructures*, 122, 124–139. Available from: https://doi.org/10.1016/j.spmi.2018.08.015

43 Ohira, T., Kawamura, M., Iida, Y. & Nakagawa, Z. (2008) Antibacterial Characteristics of MgO-ZnO Solid Solution with Different Chemical Compositions. *Transactions of the Materials Research Society of Japan*, 33(4), 1273–1276. Available from: https://doi.org/10.14723/tmrsj.33.1273

44 Othman, Z.J. & Matoussi, A. (2016) Morphological and optical studies of zinc oxide doped MgO. *Journal of Alloys and Compounds*, 671, 366–371. Available from: Available from: https://doi.org/10.1016/j.jallcom.2016.02.069

45 Pacchioni, G. (2001) 3-Theory of point defects at the MgO surface. In: Woodruff, D.P. (Ed.) *Nanocatalysis*, pp. 94-135. Available from: https://doi.org/10.1016/S1571-0785(01)80023-7

46 Pacchioni, G. & Freund, H. (2013) Electron transfer at oxide surfaces. The MgO paradigm: From defects to ultrathin films. *Chemical Reviews*, 113(6), 4035-4072. Available from: https://doi.org/10.1021/cr3002017

47 Panin, G.N., Baranov, A.N., Oh, Y.J., Kang, T.W. & Kim, T.W. (2005) Effect of thermal annealing on the structural and the optical properties of ZnO/MgO nanostructures. *Journal of Crystal Growth*, 279(3-4), 494–500. Available from: https://doi.org/10.1016/j.jcrysgro.2005.02.068

48 Pathak, N., Ghosh, P.S., Gupta, S.K., Kadam, R.M. & Arya, A. (2016) Defects induced changes in the electronic structures of MgO and their correlation with the optical properties: A special case of electron-hole recombination from the conduction band. *RSC Advances*, 6, 96398–96415. Available from: https://doi.org/10.1039/c6ra21065a

49 Płóciennik, P., Guichaoua, D., Zawadzka, A., Korcala, A., Strzelecki, J., Trzaska, P. & Sahraoui, B. (2016) Optical properties of MgO thin films grown by laser ablation technique. *Optical and Quantum Electronics*, 48. Available from: https://doi.org/10.1007/s11082-016-0536-8

50 Prasad, C., Rajagopal Reddy, V., Choi, C.-J. (2017) Electrical and carrier transport properties of the Au/Y2O3/n-GaN metal-insulator-semiconductor (MIS) diode with rare-earth oxide interlayer. *Applied Physics A*, 123. Available from: https://doi.org/10.1007/s00339-017-0894-5

51 Priyadarshini, B., Sahoo, B.P., Sahoo, T. & Sahoo, T.R. (2021) Effect of Zn doping on dielectric properties of MgO nanoparticles synthesized by microwave-assisted combustion route. *Materials Letter*, 304, 130645. Available from: https://doi.org/10.1016/j.matlet.2021.130645

52 P., S.P. (2020) Structural and Electrical Studies on Zinc Added Magnesium Oxide Nanoparticles. *Journal of Physical Science*, 31, 73–86. Available from: https://doi.org/10.21315/jps2020.31.3.6

53 Qin, L., Zhao, J., & Zou, X. (2009) Synthesis and morphology evolution of tubular tetrapod MgO by thermal evaporation. *Materials Chemistry and Physics*, *113*(1), 468–473. Available from: https://doi.org/10.1016/j.matchemphys.2008.07.115

54 Rajesh Kumar, B., & Subba Rao, T. (2011) High-k Gate Dielectrics of Thin Films with its Technological Applications-A Review. In: *International Journal of Pure and Applied Sciences and Technology*, 4(2), 105-114. Available online at: www.ijopaasat.in

55 Rathore, D. & Arora, S. (2020) Investigation of Structural and Optical Properties of (ZnO)x-(MgO)1-x (x=1.0, 0.75, 0.50, 0.20, 0.10) Nano crystalline Thin Films. *SKIT Research Journal*, *10*(1), 16-19. Available from: https://doi.org/10.47904/IJSKIT.10.1.2020.16-19

56 Robertson, J. (2004) High dielectric constant oxides. *EPJ Applied Physics*, 28(3), 265-291. Available from: https://doi.org/10.1051/epjap:2004206

57 Rodnyi, P. A. & Khodyuk, I. V. (2011) Optical and Luminescence Properties of Zinc Oxide. In: *Optics and Spectroscopy*, 111(5), 776-785. Available from: http://doi.org/10.1134/S0030400X11120216

58 Rostron, P., Gaber, S. & Gaber, D. (2016) Raman Spectroscopy, Review. *International Journal of Engineering and Technical Research*, 6(1), 50-64.

59 Saadi, H., Benzarti, Z., Sanguino, P., Pina, J., Abdelmoula, N. & de Melo, J.S.S. (2023) Enhancing the electrical conductivity and the dielectric features of ZnO nanoparticles through Co doping effect for energy storage applications. *Journal of Materials Science: Materials in Electronics*, 34, 1–16. Available from: https://doi.org/10.1007/s10854-022-09470-5

60 Sciau, Ph. (2016) 2 - Transmission Electron Microscopy: Emerging Investigations for Cultural Heritage Materials. In: P. W. Hawkes (Ed.), *Advances in Imaging and Electron Physics* 198, pp. 43–67. Available from: https://doi.org/10.1016/bs.aiep.2016.09.002

61 Seeger, A., Lunkenheimer, P., Hemberger, J., Mukhin, A.A., Ivanov, Y., Balbashov, A.M. & Loidl, A. (1999) Charge carrier localization in La 1−x Sr x MnO 3 investigated by ac conductivity measurements. *Journal of Physics: Condensed Matter*, 11, 3273. Available from: https://doi.org/10.1088/0953-8984/11/16/009

62 Selvam, N.C.S., Kumar, R.T., Kennedy, L.J. & Vijaya, J.J. (2011) Comparative study of microwave and conventional methods for the preparation and optical properties of novel MgO-micro and nano-structures. *Journal of Alloys and Compounds*, 509(41), 9809–9815. Available from: https://doi.org/10.1016/j.jallcom.2011.08.032

63 Sharma, A., Arya, S., Singh, B., Prerna, Tomar, A., Singh, S. & Sharma, R. (2020) Sol-Gel Synthesis of Zn Doped MgO Nanoparticles and Their Applications. *Integrated Ferroelectrics: Proceedings of International Conference on Nano-structured materials and Devices*, 205, 14–25. Available from: https://doi.org/10.1080/10584587.2019.1674993

64 Sharma, U. & Jeevanandam, P. (2015) Synthesis of Zn^{2+}-doped MgO nanoparticles using substituted brucite precursors and studies on their optical properties. *Journal of Solgel Science and Technology*, 75, 635–648. Available from: https://doi.org/10.1007/s10971-015-3734-0

65 Sharma, U., Kumar, G., Mishra, S., Thomas, R. (2022) Advancement of Gate Oxides from SiO_2 to High-k Dielectrics in Microprocessor and Memory, in: Journal of Physics: Conference Series. Institute of Physics. https://doi.org/10.1088/1742-6596/2267/1/012142

66 Shindo, D. & Hiraga, K. (1998) Practice of High-Resolution Electron Microscopy. In: D. Shindo & K. Hiraga (Eds.), *High-Resolution Electron Microscopy for Materials Science*. Springer, Japan, pp. 17–39. https://doi.org/10.1007/978-4-431-68422-0_2

67 Sichelschmidt, J., Paraskevopoulos, M., Brando, M., Wehn, R., Ivannikov, D., Mayr, F., Pucher, K., Hemberger, J., Pimenov, A., Krug Von Nidda, H.-A., Lunkenheimer, P., Ivanov, V.Y., Mukhin, A.A., Balbashov, A.M. & Loidl, A. (2001) Magnetic, electronic, dielectric and optical properties of Pr(Ca:Sr)MnO_3. *The European Physical Journal B-Condensed Matter and Complex systems*, 20, 7-17. Available from: https://doi.org/10.1007/s100510170280

68 Smith, D. J. (1997) The realization of atomic resolution with the electron microscope. In: *Reports of Progress in Physics*, 60(12), 1513-1580. Available from: https://doi.org/10.1088/0034-4885/60/12/002

69 Smith, J.G., Naruse, J., Hiramatsu, H. & Siegel, D.J. (2017) Intrinsic Conductivity in Magnesium-Oxygen Battery Discharge Products: MgO and MgO2. *Chemistry of*

Materials 29, 3152–3163. Available from: https://doi.org/10.1021/acs.chemmater.7b00217

70 Soma, H. & Uchino, T. (2017) Blue and orange photoluminescence and surface band-gap narrowing in lithium-doped MgO microcrystals. *Journal of Physical Chemistry C*, 121, 1884–1892. Available from: https://doi.org/10.1021/acs.jpcc.6b12177

71 Stankic, S., Müller, M., Diwald, O., Sterrer, M., Knözinger, E. & Bernardi, J. (2005) Size-Dependent Optical Properties of MgO Nanocubes. *Angewandte Chemie (International Ed. in English)*, 44, 4917–4920. Available from: https://doi.org/10.1002/anie.200500663

72 Sternig, A., Stankic, S., Müller, M., Siedl, N. & Diwald, O. (2012) Surface exciton separation in photoexcited MgO nanocube powders. *Nanoscale*, 4, 7494–7500. Available from: https://doi.org/10.1039/c2nr31844j

73 Sun, L., Zhang, R., Wang, Z., Cao, E., Zhang, Y. & Ju, L. (2016) Microstructure, dielectric properties and impedance spectroscopy of Ni doped CaCu3Ti4O12 ceramics. *RSC Advances*, 6, 55984–55989. Available from: https://doi.org/10.1039/c6ra07726a

74 Sushko, P. V., Gavartin, J.L. & Shluger, A.L. (2002) Electronic properties of structural defects at the MgO (001) surface. *The Journal of Physical Chemistry B*, 106, 2269–2276. Available from: https://doi.org/10.1021/jp0129481

75 Tamizh, K., Rathnakumari, S.M., Priya, M. & Suresh Kumar, P. (2014) Shape Transition Effect of Temperature on MgO Nanostructures and its Optical Properties. *International Journal of Scientific & Engineering Research*, 5(3), 60-64.

76 Tipaldi, C.F. & Gabrusenoks, J. (2022) Lattice Dynamics Calculations for $Mg_{1-x}Zn_xO$ Solid Solutions. *Latvian Journal of Physics and Technical Sciences*, 59, 3–11. Available from: https://doi.org/10.2478/lpts-2022-0007

77 Vasanthi, V., Kottaisamy, M., Anitha, K. & Ramakrishnan, V. (2017) Near UV excitable yellow light emitting Zn doped MgO for WLED application. *Superlattices and Microstructures*, 106, 174–183. Available from: https://doi.org/10.1016/j.spmi.2017.03.050

78 Wang, J., Tu, Y., Yang, L. & Tolner, H. (2016) Theoretical investigation of the electronic structure and optical properties of zinc-doped magnesium oxide. *Journal of Computational Electronics*, 15, 1521–1530. Available from: https://doi.org/10.1007/s10825-016-0906-2

79 Wang, S., Liu, X. & Zhou, P. (2022) The Road for Two-Dimensional Semiconductors in Silicon Age. *Advanced Materials*, 34(48), 2106886. Available from: https://doi.org/10.1002/adma.202106886

80 Wilson, I.O. (1981) Magnesium oxide as a high-temperature insulant. *Proceedings of the institution of Electrical Engineers*, 128, 3, 159-164.

81 Wobbe, M.C.C., Kerridge, A. & Zwijnenburg, M.A. (2014) Optical excitation of MgO nanoparticles; a computational perspective. *Physical Chemistry Chemical Physics*, 16, 22052–22061. Available from: https://doi.org/10.1039/c4cp03442b

82 Xia, L., Liu, Z. & Taskinen, P. (2016) Solubility study of the halite and wurtzite solid solutions in the MgO-ZnO system within temperature range from 1000 to 1600 °C. *Journal of Alloys and Compounds*, 687, 827–832. Available from: https://doi.org/10.1016/j.jallcom.2016.06.191

83 Zhang, X., Zheng, Y., Feng, X., Han, X., Bai, Z., & Zhang, Z. (2015) Calcination temperature-dependent surface structure and physicochemical properties of magnesium oxide. *RSC Advances*, *5*(105), 86102–86112. Available from: https://doi.org/10.1039/c5ra17031a

84 Zhu, T.J., Lu, L. & Zhao, X.B. (2006) Orientation of MgO thin films grown by pulsed laser deposition. *Materials Science and Engineering: B*, 129, 96–99. https://doi.org/10.1016/j.mseb.2005.12.026

85 Zwijnenburg, M. A. (2021) The effect of particle size on the optical and electronic properties of magnesium oxide nanoparticles. *Physical Chemistry Chemical Physics*, *23*(38), 21579–21590. https://doi.org/10.1039/d1cp02683

CERTIFICATE
(SYNOPSIS APPROVAL CERTIFICATE)

This is to certify that the Synopsis for Ph.D. Thesis titled, **"STRUCTURAL, OPTICAL AND TEMPERATURE DEPENDENT DIELECTRIC STUDY OF ZINC OXIDE (ZnO) INCORPORATED MAGNESIUM OXIDE (MgO) BASED COMPOUNDS"**, submitted by **Ms. Jyotsna** to the Career Point University, Hamirpur (H.P.), India in partial fulfillment of the requirements for the degree of **DOCTOR OF PHILOSOPHY** in the Department of Physics, School of Basic & Applied Sciences, Career Point University, Hamirpur (H.P.) has been approved by the Research Advisory Committee (RAC) after an Oral Examination of the student on dated 27-06-2022.

Dr. Rajender Kumar
Associate Professor, Department of Physics
Career Point University Hamirpur (HP)
(Supervisor)

Research Advisory Committee

Dr. Naveen Thakur
Professor, Department of Physics
Career Point University Hamirpur (HP)
(Member)

Dr. Indu Sharma
Associate Professor, Department of Physics
Career Point University Hamirpur (HP)
(Member)

Dr. Kuldeep Kumar
Associate Professor, Department of Chemistry
Career Point University Hamirpur (HP)
(Member)

Dr. Naveen Thakur
Professor, Department of Physics
Career Point University Hamirpur (HP)
(Head)
Department of Physics

Dr. Kuldeep Kumar
Associate Professor, Department of Chemistry
Career Point University Hamirpur (HP)
(Associate Dean PG Studies-cum-Associate Director Research)